Inorganic Chemistry

Article

pubs.acs.org/IC

Investigation of New Alkali Bismuth Oxosulfates and Oxophosphates with Original Topologies of Oxo-Centered Units

Minfeng Lü,[†,∥] Marie Colmont,*[,†] Marielle Huvé,[†] Isabelle De Waele,[‡] Christine Terryn,[§] Almaz Aliev,[†] and Olivier Mentré*[,†]

[†]Université Lille Nord de France, UMR 8181 CNRS, Unité de Catalyse et de Chimie du Solide (UCCS USTL), F-59655 Villeneuve d'Ascq, France

[‡]University Nord de France, Lille1, LASIR (UMR CNRS A8516), 59655 Villeneuve d'Ascq Cedex, France

[§]Plateforme Imagerie Cellulaire et Tissulaire, 51 Rue Cognacq-Jay, 51100 Reims, France

[∥]State Key Laboratory of Rare Earth Resource Utilization, Changchun Institute of Applied Chemistry, Chinese Academy of Sciences, Changchun 130022, P. R. China

Supporting Information

ABSTRACT: Two new alkali bismuth oxosulfates, $[Bi_{12}O_{15}]Li_2(SO_4)_4$ (**I**) and $[Bi_7K_2O_8]K(SO_4)_4$ (**II**), have been synthesized by heating a mixture of Bi_2O_3, $CuSO_4 5H_2O$, and A_2CO_3 (A = Li, K), and characterized by single crystal XRD, transmission electron microscopy, and multiphoton SHG and IR spectroscopy. In the above formula the $[Bi_xO_y]$ subunits denote the 3D-porous (**I**) or 1D-columnar (**II**) polycationic host-lattice formed of edge-sharing OBi_4 or $O(Bi,K)_4$ oxocenterd tetrahedra. The SO_4^{2-} groups and alkali ions are arranged into channels in the interstices leading to original opened crystal structures for these two first reported alkali oxo-bismuth sulfates. The strong adaptability of the oxocentered framework is demonstrated by the possibility of preparing single crystals of $[Bi_{8.73}K_{0.27}O_8]K_{1.54}(PO_4)_4$ (**III**) whose crystal structure is similar to those of **II** with disorder between OBi_4 and $O(Bi_3,K)$ tetrahedra and different channel occupancy due to the aliovalent replacement of SO_4^{2-} for PO_4^{3-}.

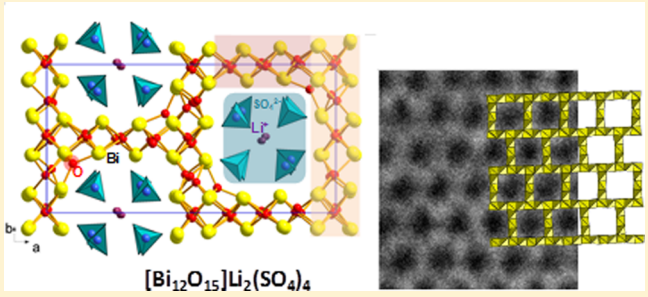

INTRODUCTION

The search for new materials with innovative architectures is the driving force of solid state chemists, especially new materials with unexpected properties (electrical, catalytic, magnetism, optical, and so forth). At this level, the crystal chemistry of bismuth oxides and oxosalts is very rich since it is generally related to complex polycations formed of oxocentered tetrahedra as detailed in ref 1. The resulting frameworks derive from the oxygen-deficient fluorite structure of δ-Bi_2O_3 in which the condensation of vacant $O(Bi,\square)_4$ tetrahedra is maximal leading to a compact 3D structure. Indeed, we recall that this phase exhibits so far the most excellent oxide ion conducting properties at high temperature.[2] Most of the inorganic chemistry of bismuth oxosalts, for instance after incorporating PO_4^{3-}, WO_4^{2-}, MoO_4^{2-}, CrO_4^{2-}, or SO_4^{2-} polyanions in Bi_2O_3,[2−9] originates from attempts to stabilize the high temperature defect fluorite type to reach performant anionic conductors at lower temperatures[2,10] although their conductivity performances are not as high as expected.[11−16] At least it is clear from their crystal chemistry that it is often related to the parent fluorite type where oxo-anions are incorporated. The structural analogy was recently demonstrated in several mixed Bi^{3+}/M^{n+} oxophosphates.[17,18] In this large family, the remaining oxocentered $O(Bi,M)_4$ tetrahedra can be separated or condensed into zero-dimensional (0D), one-dimensional (1D), two-dimensional (2D), and three-dimensional (3D) frameworks surrounded by isolated phosphate groups but conserving the initial fluorite organization. It forms a rich playground for finding innovative architecture with potential physical properties.

To tackle new compounds, one possibility consists of the diversification of XO_4 oxoanions such as SO_4^{2-}. Compared to the number of phases reported with PO_4^{3-} anions, the charge difference is expected to modify the oxocentered framework leading recently to very interesting magnetic topologies in $[Bi_2CoO_3](SO_4)$ and $[Bi_{6.3}Cu_{1.6}O_8](SO_4)_3$.[19] In addition, the number of referenced bismuth sulfate in the literature is rather narrow, opening the door to new hypothetical structures.

Among these oxosalts, the $Bi^{3+}-O^{2-}-SO_4^{2-}$ ternary system included 10 different bismuth oxosulfates[8,9,20−23] in addition to Bi_2O_3[24] and $Bi_2(S_2O_7)_3$.[25] The Bi:SO_4 ratio in each compound varies from 0.33:1 to 14:1. Almost all of them were obtained after pyrolysis of $Bi_2(SO_4)_3$. $Bi_2O_2SO_4$ was the first reported in 1965.[20−23] With the loss of additional SO_3, the subsequent pyrolysis products changed into $(Bi_{26}O_{27})(SO_4)_{12}$ and $(Bi_{14}O_{16})(SO_4)_5$.[21] At this stage, two important compounds with lower

Received: July 30, 2014
Published: October 31, 2014

   dx.doi.org/10.1021/ic501776h | *Inorg. Chem.* 2014, 53, 12058−12065

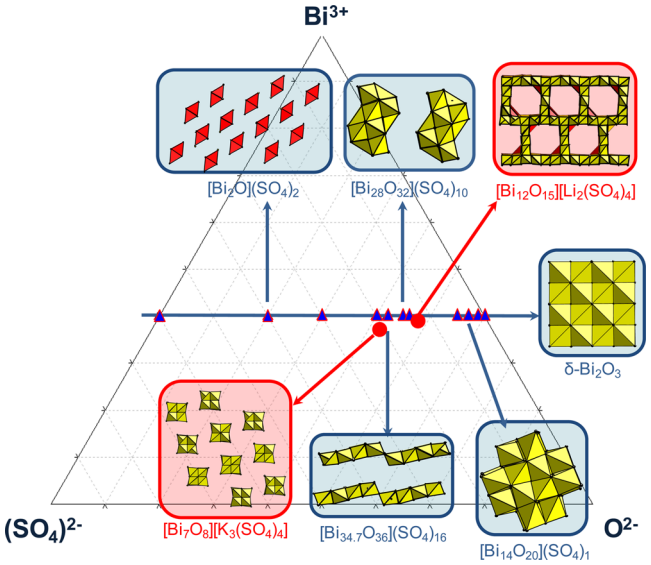

Figure 1. Phase diagram in the $Bi^{3+}-O^{2-}-SO_4^{2-}$ system. Oxocentered crystal structures enhanced a constant amount of bismuth: 40%. OBi_4 entities are drawn in yellow and OBi_3 in red.

SO_4 content were reported: (1) $(Bi_8O_{11})(SO_4)$ characterized by a complex low temperature phase and defected fluorite structure high temperature phase[8] and (2) $(Bi_{14}O_{20})(SO_4)$ which adopts a commensurate superstructure of the cubic fluorite subcell.[7] These structures are composed of a discrete ratio of SO_4^{2-} groups inside the parent fluorite-related region with edge sharing of OBi_4 tetrahedra.

The ternary $Bi^{3+}-SO_4^{2-}-O^{2-}$ system drawn on Figure 1 displays all crystal structures referenced in the literature. All compositions are aligned in the phase diagram with respect to the final electroneutrality of the compound. Most representative oxocentered frameworks are represented (OBi_3 triangles in red versus OBi_4 tetrahedra in yellow) and show an increasing connectivity between the elementary units upon increasing the bismuth content.

With the ulterior motivation of preparing novel bismuth oxosulfates, a flux crystal growth route was entertained, using Li_2CO_3 and K_2CO_3 as fluxes. It finally leads to the preparation of two new compounds with interstitial alkali arranged in SO_4 channels: (**I**) the porous $[Bi_{12}O_{15}][Li_2(SO_4)_4]$ and (**II**) the columnar $[Bi_7K_2O_8][K(SO_4)_4]$. Compound **III**, $[Bi_{8.73}K_{0.27}O_8]$-$[K_{1.54}(PO_4)_4]$, strongly related to **II**, was prepared to validate the adaptability of such crystal structures to versatile XO_4^{n-} counteranions.

EXPERIMENTAL SECTION

Synthesis: $[Bi_{12}O_{15}][Li_2(SO_4)_4]$ (I). Single crystals of **I** have been obtained from the slow cooling of a mixture of Bi_2O_3/ $CuSO_4 \cdot 5H_2O$/Li_2CO_3 in the molar ratio 2:2:1. The mixtures were put into a gold tube and vacuum sealed in quartz tubes after thorough grinding. Heat treatments were performed at 1253 K for 2.5 h and quickly dropped to 973 K, and finally cooled down to 773 K for 66.7 h (3 K/h). Qualitative EDX analyses of isolated transparent pellet shaped crystals indicate the presence of both Bi and S as constituting element. Li cation was not detectable by this method.

$[Bi_7K_2O_8][K(SO_4)_4]$ (II). The transparent brick crystals were found in the melt of the mixture of Bi_2O_3/ $CuSO_4 \cdot 5H_2O$/K_2CO_3 with molar ratio 2:1:1. After thorough grinding and mixing, the above-mentioned sample was loaded into gold tubes, and then vacuum sealed in silica

Table 1. Crystal Data, Measurement, and Structural Refinement Parameters of $[Bi_{12}O_{15}][Li_2(SO_4)_4]$, $[Bi_7K_2O_8][K(SO_4)_4]$, and $[Bi_{8.73}K_{0.27}O_8][K_{1.54}(PO_4)_4]$

	$[Bi_{12}O_{15}][Li_2(SO_4)_4]$ (**I**)	$[Bi_7K_2O_8][K(SO_4)_4]$ (**II**)	$[Bi_{8.73}K_{0.27}O_8][K_{1.54}(PO_4)_4]$ (**III**)
Crystal Data			
cryst symmetry space group	orthorhombic	monoclinic	tetragonal
	$P2_12_12_1$	$C2/c$	$I4/m$
a (Å)	23.0661(10)	28.5219(8)	13.977(2)
b (Å)	11.4330(5)	11.4600(3)	
c (Å)	11.2237(5)	20.0843(6)	5.7846(7)
β (deg)		133.3070(9)	
V (Å^3)	2959.8(2)	4777.1(2)	1130.1(2)
Z	4	8	2
D_x (g/cm^3)	7.0573	5.8166	7.059
μ (mm^{-1}) (for λ Kα = 0.7107 Å)	71.455	52.359	68.427
appearance	transparent, colorless	transparent, colorless	transparent, colorless
Data Collection			
λ(Mo Kα) (Å)	0.710 73	0.710 73	0.710 73
scan mode	ω and φ	ω and φ	ω and φ
$\theta_{(min-max)}$ (deg)	1.77−33.1	1.96−33.16	2.06−33.37
R(int) (%)	6.64	6.27	3.6
recording reciprocal space	$-35 \le h \le 35$	$-43 \le h \le 43$	$-20 \le h \le 21$
	$-15 \le k \le 17$	$-17 \le k \le 17$	$-13 \le k \le 20$
	$-17 \le l \le 17$	$-27 \le l \le 27$	$-5 \le l \le 8$
Refinement			
indep obsd/indep all (obsd = $I > 3\sigma(I)$)	9599, 11 128	3204, 5246	918, 1101
no. refined params	269	224	61
refin method	F	F	F
R1(F^2)(obsd)/R1(F^2)(all)	0.0646/0.0785	0.0350/0.0679	0.070/0.076
wR2(F^2)(obsd)/wR2(F^2)(all)	0.0725/0.0736	0.0484/0.0549	0.0756/0.0786
$\Delta\rho_{max}/\Delta\rho_{min}$ (e Å^{-3})	15.66/−13.19	2.98/−2.29	6.49/−10.11

dx.doi.org/10.1021/ic501776h | Inorg. Chem. 2014, 53, 12058−12065

tubes. Heat treatments were performed at 1253 K for 2.5 h and quickly dropped to 973 K, and finally cooled down to 773 K at the rate of 3K/h. A qualitative EDX analysis indicated the presence of Bi, K, and S as constituting elements.

$[Bi_{8.73}K_{0.27}O_8][K_{1.54}(PO_4)_4]$ (III). Single crystals of $[Bi_{8.73}K_{0.27}O_8]$-$[K_{1.54}(PO_4)_4]$ were found in a polyphasic residue obtained as following: the mixture $0.5K_2CO_3/2.5Bi_2O_3/2(NH_4)_2HPO_4$ was ground and loaded into a gold crucible which was heated up to 1173 K (rate 50 K/h), and then left for 10 h and cooled down slowly to 873 K (rate 3 K/h). Finally, the furnace was switched off. The reaction was performed in air. A qualitative EDX analysis indicated the presence of Bi, K, and P as constituting elements.

Single Crystal X-ray Diffraction. The single crystal XRD data of all the investigated samples have been collected using a Bruker Apex Duo diffractometer with a Mo IμS microfocus tube (λ = 0.710 73 Å). The intensity data have been extracted from the collected frames using the program SAINT-Plus 6.02.[26] The lattice parameters have been refined from the complete data set. Absorption corrections have been performed using multiscan methods using SADABS.[27] The data collection and pertinent data of the refinements for all single crystals studied in this work are gathered in Table 1.

Transmission Electron Microscopy. Studies were performed on a FEI Tecnai G2-20 twin TEM microscope. The polycrystalline materials (prepared as detailed above) were crushed and dropped in the form of aqueous or alcohol suspensions on carbon-supported copper grids followed by evaporation under ambient conditions. The computer simulated HREM images were calculated using the JEMS program.[28]

Conductivity Measurements. Electrical measurements were performed on $[Bi_{12}O_{15}][Li_2(SO_4)_4]$ by impedance spectroscopy between room temperature and 700 °C using a Solartron 1260 impedance analyzer with a 500 mV amplitude signal over the 0.1 Hz to 10 MHz frequency range. Silver paste was painted at both sides of a single crystal (400 μm long) externally to the *c*-direction. All impedance diagrams were normalized using the thickness/surface geometrical factor. Fitting of impedance spectra were performed using Zview.[29] using typical RC circles.

Multiphoton SHG Microscopy. In this study, a laser scanning microscope LSM 710 NLO Zeiss (Jena, Germany) was used as implemented at the Plateforme d'Imagerie Cellulaire et Tissulaire, Reims, France. Excitation was provided by a CHAMELEON femtosecond titanium-sapphire laser (Coherent, Santa Clara, CA) set at 860 nm, tuning the power until SHG was detected. Samples were imaged with a 20× , 0.8 NA objective lens. Emitted signal of SHG was collected with a bandpass filter (420−440 nm) . The analyzed zone is performed by pixels of 0.55 × 0.55 μm^2.

RESULTS AND DISCUSSION

Crystal Structure of Compound (I). A colorless single crystal was isolated and mounted on a glass fiber. The XRD data collection and structural refinement are presented in Table 1. $[Bi_{12}O_{15}][Li_2(SO_4)_4]$ crystallized in an orthorhombic unit cell with lattice parameters of a = 23.0661(10) Å, b = 11.4330(5) Å, and c = 11.2237(5) Å. We note that, in spite of difficulties to determine the true space group and to solve the crystal structure in orthorhombic, the merging in different Laue group symmetry of the reflections does not show any improvement between the three monoclinic settings (R_{int} ∼ 5.4% to 6.4% along the three axes in the 2/*m* Laue class) and the orthorhombic symmetry (R_{int} = 6.64% using the *mmm* Laue class). It was finally solved using the charge flipping program[29] and refined using Jana 2006[30] in the $P2_12_12_1$ noncentrosymmetric space group while the Addsym application implemented in PLATON[31] refuted a more symmetrical solution, as confirmed by our nonconverging tests in centrosymmetric space groups. We also tried monoclinic $P2_1$ symmetries with the 2-fold axis subsequentelly set along *a*, *b*, and *c*. The solutions obtained were essentially the same as that in $P2_12_12_1$ in any cases with a much larger number of refined parameters. The noncentrosymmetric space group was further proved by SHG measurements, dealing with a rather thick crystal. Only thin edges of the crystal show a significant SHG signal, as shown in blue on the corresponding image, Figure 2a. In the current setting

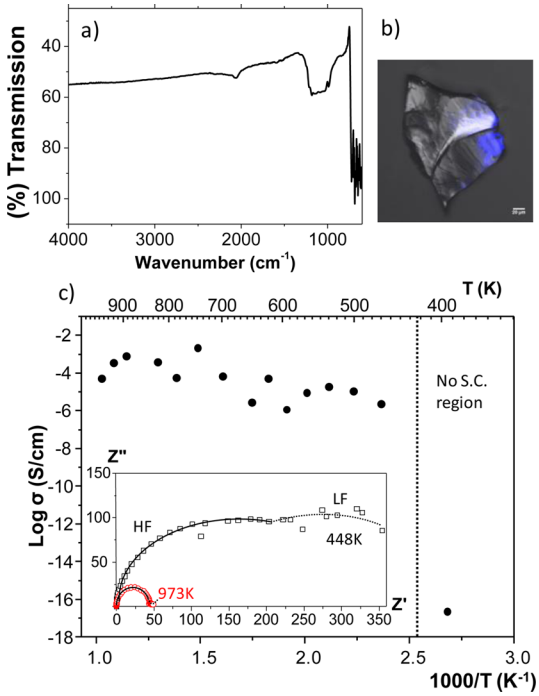

Figure 2. (a) FT-IR spectrum of $[Bi_{12}O_{15}][Li_2(SO_4)_4]$. No evidence for proton was revealed. (b) Transmission image of a crystal of $[Bi_{12}O_{15}][Li_2(SO_4)_4]$: emitting surface ($\lambda_{em}$ = 420−440 nm, λ_{em} = 860 nm). (c) Arrhenius plot of the conductivity of the $[Bi_{12}O_{15}]$-$[Li_2(SO_4)_4]$. Inset: Nyquist plots for the measurements at 448 and 973 K with indication of the relaxation frequency domains (HF, high frequency; LF, low frequency).

the detected SHG signal is maximal in the horizontal plane (below the crystal) that corresponds to the laser polarization, which reduces the detection for thick and irregular samples due to high absorption. In addition the refinement of twinned racemic domains (ratio: ∼40%/60%) suggests the possibility for local SHG quenching. Atomic and thermal parameters were refined for the 12 independent Bi and 4 independent S positions. For the 31 oxygen positions, only isotropic thermal parameters have been considered. At this stage, the refined formula is not neutral ($[Bi_{12}O_{15}][(SO_4)_4]$) which suggests two possibilities: (1) Taking into account the BVS calculated on inner SO_4 corners, far to −2 we may either deal with SO_4H groups. The absence of band at 3500 cm^{-1} on infrared spectrum discards this possibility, Figure 2a. (2) Either of the SO_4 groups arranged into channels host cations with a low XRD contrast, i.e., Li^+ ions from the Li_2CO_3 flux. The study of the Fourier difference maps clearly indicates the presence of residual electron density in the corresponding square channels, as shown on Figure 3c. Due to the small contribution of Li^+ ions in a context of heavy atoms, Li^+ ions were fixed, but diffuse residual density along the *c*-axis may suggest disorder or possible diffusion paths as discussed below. The final residual factors converged to R1 = 0.0646 and wR = 0.0725 for 269 refined parameters and 11 128 used reflections ($I > 3\sigma(I)$).

dx.doi.org/10.1021/ic501776h | Inorg. Chem. 2014, 53, 12058−12065

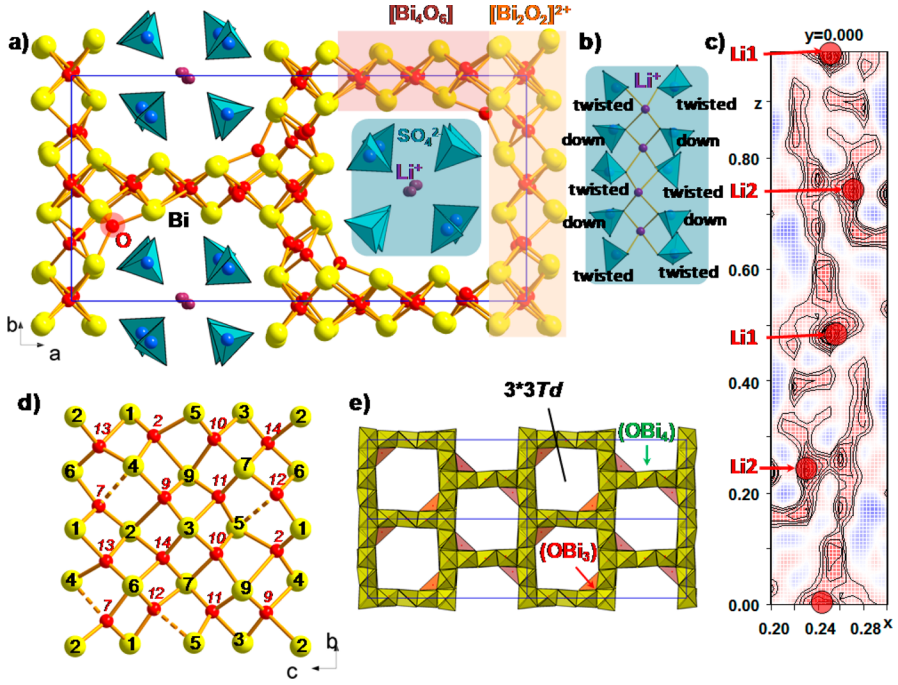

Figure 3. (a) Projection of the structure of $[Bi_{12}O_{15}][Li_2(SO_4)_4]$ along the *c* axis. Isolated SO_4^{2-} tetrahedron is drawn in light blue. (b) Projection of a slab of $[Li_2(SO_4)_4]_{channel}$ along (010). (c) Fourier difference along (*x*, *z*) in the tunnel. Residual density corresponds to the Li contributions. (d) Projection of a slab of part of $[Bi_{12}O_{15}]^{6+}$ blocks on the ($^1/_2$00) plane. (e) Porous 3D-networks of OBi_4 tetrahedra in yellow (the connection of OBi_3 triangle is highlighted in red).

Table 2. BVS of $[Bi_{12}O_{15}]Li_2(SO_4)_4]$, $[Bi_7K_2O_8][K(SO_4)_4]$, and $[Bi_{8.73}K_{0.27}O_8][K_{1.54}(PO_4)_4]$[a]

$[Bi_{12}O_{15}][Li_2(SO_4)_4]$				$[Bi_7K_2O_8][K(SO_4)_4]$				$[Bi_{8.73}K_{0.27}O_8][K_{1.54}(PO_4)_4]$			
atom	V_{Bi*}	V_{S*}	V_{Li*}	atom	V_{Bi*}	V_{K*}	V_{S*}	atom	V_{Bi*}	V_{K*}	V_{S*}
Bi1	3.01			Bi1	2.86			Bi1	3.07(8)		
Bi2	2.81			Bi2	2.91			Bi2	2.52(5)		
Bi3	2.68			Bi3	3.00			Bi3	2.65(11)		
Bi4	2.95			Bi4	3.08			K3		3.2(7)	
Bi5	2.88			Bi5	3.10			K1		1.22(5)	
Bi6	2.93			Bi6	3.02			P1			5.3(3)
Bi7	2.89			Bi7	3.10						
Bi8	3.02			Bi8	2.95						
Bi9	2.97			K1		1.10					
Bi10	3.14			K2		0.99					
Bi11	2.86			K3		1.04					
Bi12	3.01			S1			6.27				
S1		7.2		S2			6.17				
S2		7.1		S3			6.24				
S3		7.1		S4			7.10				
S4		7.9									
Li1			0.92								
Li2			0.81								

[a] (*R*, *b*) parameters being for Bi^{3+}—O (2.094, 0.37), Li^+—O (1.466, 0.37), K^+—O (2.132, 0.37), S^{6+}—O (1.624,0.37), P^{5+}—O (1.604, 0.37).

The refined atomic positions and anisotropic displacement parameters are given in Supporting Information Tables S1 and S2, respectively. The pertinent distances are listed in Supporting Information Table S3. We note a strong residual density close to the atom Bi3. It most probably arises from local weak disorder due to antiphase boundaries. It could be lowered by splitting the Bi3 site, but more than 3 positions are necessary. We prefer here to present the most ideal model.

Novel Porous Network. Supporting Information Table S3 gives selected distances and angles within the structure of $[Bi_{12}O_{15}][Li_2(SO_4)_4]$. Bismuth atoms are coordinated by, respectively, 4 (Bi10), 5 (Bi1), 7 (Bi2 and Bi5), and 6 (for all other Bi) oxygen atoms. The Bi—O distances range from 2.11 to 3.15 Å, which lead to rather good BVS values close to +3 for Bi^{3+}, using the parameters from ref 32 as listed in Table 2. The shortest O—O distance outside the SO_4^{2-} groups is 2.59(2) Å between O(3) and O(15), which does not differ very much from those in $Bi_{34(2/3)}O_{36}(SO_4)_{16}$, 2.62(10) Å bond.[21] However, SO_4^{2-} groups show a significant disorder, especially around S(2) and S(4) centers. The O2b—S2—O2c angle is

dx.doi.org/10.1021/ic501776h | *Inorg. Chem.* 2014, 53, 12058−12065

126°, which deviates considerably from the ideal angle value. Also, the shortest O−S distance is 1.26(2) Å for O4b−S(4) which pictures inaccuracy on the localization of the SO_4 groups, at the origin of great BVS values for S (see Table 2). However, we prefer not to constrain S−O distances for a better observation of Li electron density. Between the square channels formed by the SO_4^{2-} groups, each Li^+ cation is coordinated by four oxygen at distances between 1.90(4) and 2.20(12) (Figure 3b) Å in the form of a slightly deformed edge-shared tetrahedra elongated along *c*-axis. The Li−O distances are similar to those observed in $[Bi_4O_4][BiO]_4Cu_1Li_2(AsO_4)_4$.[17] One notes that the number of Li^+ cations per tunnels (along the $c \sim 11.2$ Å period) is equal to four. A projection of the described structure is given in Figure 3a. Clues for the noncentrosymmetric (NCS) symmetry were given by the fine observation of the SO_4 orientations in the tunnels that should contain an inversion center in any supposed centrosymmetric models. Clearly, in a same tunnel only "down" and "twisted" SO_4 exist but no "up" orientations were refined (i.e., the image of "down" SO_4 in case of inversion center), see Figure 3a. It reinforces the validity of the proposed space group. Similar topology of PO_4 tetrahedra bordering a cationic channel was already evidenced in the NCS $[Bi_{18}Zn_{10}O_{21}][Zn_5(PO_4)_{14}]$,[33] which crystallizes in the *I*2*mb* space group.

This crystal structure displays a new topology of OBi_4 building blocks connected together by edge-sharing. It forms a complex crossing network $[Bi_{12}O_{15}]^{6+}$ framework, surrounded by isolated SO_4^{2-} tetrahedral hosting Li^+ cations. Figure 3b shows the channel walls projected along the normal to the *c*-axis. $[Bi_{12}O_{15}]^{6+}$ blocks can be divided by infinite $[Bi_2O_2]^{2+}$ layers parallel to *b* capped by $[Bi_4O_6]$ pillars parallel to *a* every three OBi_4 tetrahedra (Figure 3d). Half of the intersections between the layers the pillars are stabilized by additional O atoms in OBi_3 triangles (Figure 3e). It creates a dense packing of 1D-cavities parallel to *c* axis which contain the SO_4 tetrahedra. The Li^+ ions take place at the middle of the square channels formed by the latter SO_4^{2-} anions.

Related oxocentered lattices with similar formula $[Bi_{12}O_{15}]^{6+}$ have already been observed in ref 34: $[Bi_{12}O_{15}][Cl_6]$ with 2 × 2 × 2 *Td* triangular pores, formed by condensed oxocentered ribbons. Here the *Td* notation denotes OBi_4 tetrahedra. In the title compound, the porous network displays square channels with a 3 × 3 *Td* section. The [001] TEM image (Figure 4) gives a real-space view of the arrangement between the square tunnels in agreement with the refined model. The superimposition of the structure is positioned with the help of a simulation using JEMS software.[28] It allows the use of a different defocus to observe the oxocentered framework with various image contrasts. To date, our attempts to prepare the corresponding powder sample starting from Bi_2O_3/Li_2CO_3/$(NH_4)_2SO_4$ precursors systematically failed, leading to a majority of $[Bi_{28}O_{32}][SO_4]_{10}$ (see Supporting Information Table S4).

Due to the particular electron density maps along the Li^+ channels discussed above, we performed a spectroscopic impedance analysis on a single crystal of $[Bi_{12}O_{15}][Li_2(SO_4)_4]$. The crystals are needle-shaped with the long dimension corresponding to the *c*-direction, as shown by our face indexation. It was collected under conditions given in the Experimental Section. Nyquist plots show more or less well-defined semicircles above 125 °C, Figure 2c. We have considered that the first contribution at higher frequency corresponds to the bulk conductivity. After normalization by the shape factor, we extracted

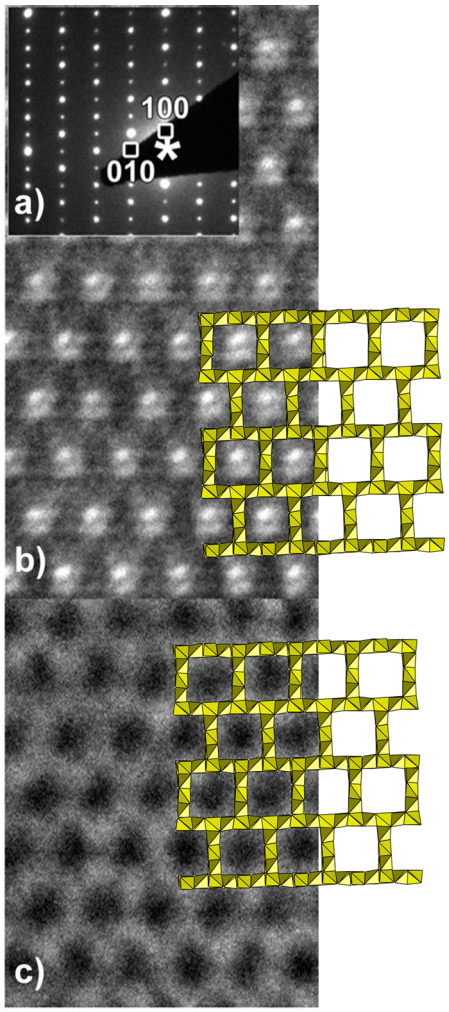

Figure 4. TEM images for compound **I**: (a) [001] electron diffraction zone axis pattern (EDZAP), (b, c) corresponding TEM image for two defocus value with the projected structure along the *c* axis. (b) The white dots indicate the position of the $[Li_2(SO_4)_4]$ channels between the $[Bi_{12}O_{15}]^{6+}$ blocks whereas in part c the light contrast is attributed to $[Bi_{12}O_{15}]^{6+}$blocks.

conductivity σ-values plotted as $\log(\sigma)$ versus $1000/T$ on Figure 2c. However, difficulties to extrapolate the semicircle intersection were frequent, at the origin of the distribution of points in Figure 2c. It was not possible to extract a meaningful activation energy from this plot, but at least one can announce conductivity between 10^{-6} and 10^{-3} S cm^{-1} between 125 and 700 °C. These low values refute any efficient Li^+ transport even on heating, accordingly with the strong bonding between SO_4^{2-} and Li^+ species.

Compound II. $[Bi_7K_2O_8][K(SO_4)_4]$ crystallizes in a monoclinic unit cell with lattice parameters $a = 28.5219(8)$ Å, $b = 11.4600(3)$ Å, $c = 20.0843(6)$ Å, $\beta = 133.3070(9)°$. The crystal structure was solved and refined in the *C*2/*c* space group, as suggested by the XPREP software.[34] However, after localization of all atoms, a slightly disordered topology emerges from overlarge values of isotropic or equivalent displacement parameters of O4b−4d involved in the highly distorted $S(4)O_4$ groups. In this structure the oxocentered tetrahedra form columns discussed below with a fully ordered −1K−Bi− sequence along the *b*-axis at the corners. One cannot fully exclude K/Bi disorder undetected by XRD that may be responsible for various

dx.doi.org/10.1021/ic501776h | *Inorg. Chem.* 2014, 53, 12058−12065

orientations of the $S(4)O_4$ group depending on the local structure. Final positional and thermal parameters are given in Supporting Information Tables S5 and S6. The final R_1 factor was 6.79 for all 5246 reflections and 3.50 for 3204 reflections.

Pillared Strucure. The structure of $[Bi_7K_2O_8][K(SO_4)_4]$ contains 1D columns of $[Bi_7K_2O_8]^{7+}$ with 2 × 2 *Td* sections infinite along the *b*-direction. The surrounding SO_4^{2-} tetrahedra form parallel channels by groups of four. K^+ ions are hosted in the square channels, leading to 8-coordinated KO_8 polyhedra. A projection of the described structure is shown in Figure 5a. The corresponding 2D-cationic network of

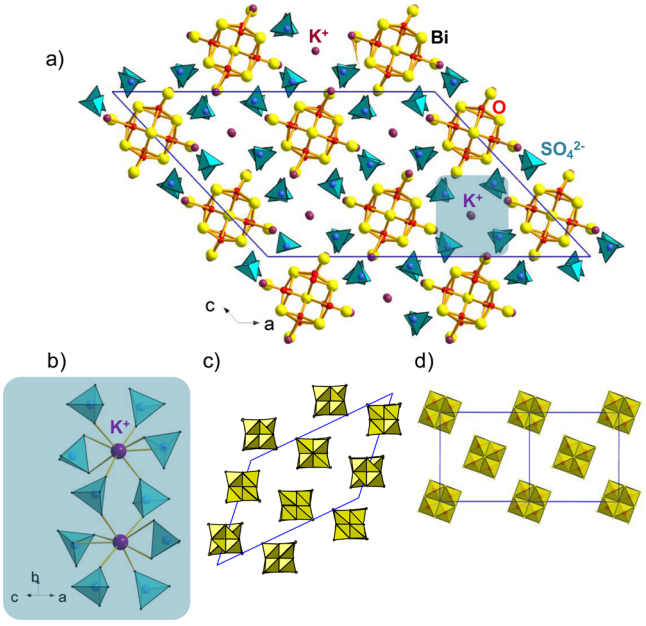

Figure 5. (a) Projection of the structure of $[Bi_7K_2O_8][K(SO_4)_4]$ along the *b* axis. Isolated SO_4^{2-} tetrahedra are drawn in light blue. (b) Projection of a slab of $[K(SO_4)_4]_{channel}$ on the $00^1/_4$ plane. (c) Isolated cationic network of $[Bi_7K_2O_8]^{7+}$ blocks in yellow compared to (d) those in $[Bi_{10}(Bi_{\sim 0.5}Cd_{\sim 0.5})_8O_{16}](Bi_{0.6}Cd_{0.8})_2(PO_4)_8$.

$[Bi_7K_2O_8]^{7+}$ is shown in Figure 5c. Once more, the [001] TEM image (Figure 7) confirmed the arrangement between the cationic part and surrounding sulfate groups in agreement with the refined model. In terms of an oxo-centered concept, the columns are formed of OBi_4 and OBi_3K_1 tetrahedra are fully ordered with distances 2.11(1) Å < O−Bi < 2.73(1) Å and 2.88(1) Å < O−K < 3.03(1) Å. Similar columnar building units have already been observed in the modulated $[Bi_{10}(Bi_{\sim 0.5}Cd_{\sim 0.5})_8O_{16}](Bi_{0.6}Cd_{0.8})_2(PO_4)_8$[34] (Figure 5d). However, in this compound Bi/Cd inside the channels and at the corners are ordered along an aperiodic period, contrarily to the present fully ordered case. It follows that PO_4^{3-} and SO_4^{2-} groups can template similar oxocenterd framework while the different charges can be balanced by the substitution of Cd^{2+} by K^+. By comparison between parts c and d of Figure 5, it is obvious that the difference of ionic radii between Cd and K induced distortions inside the columns.

Coordination and BVS Study. The coordination number around Bi1 and Bi2 is eight, compared to those of Bi3−7 which are seven. Bi8 shows a lower coordination number, i.e., five. The Bi−O distances around Bi3−Bi8 are similar, ranging from 2.11 to 2.95 Å, in contrast to Bi−O bonds in Bi1 and Bi2, with a narrow distribution of bond length, varying from 2.32 to

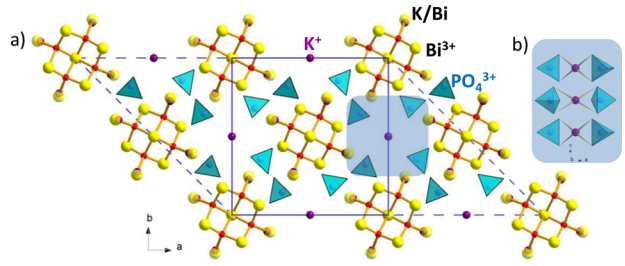

Figure 6. (a) Structure of compound **III**, $[Bi_{8.73}K_{0.27}O_8][K_{1.54}(PO_4)_4]$. Unit cells of compound **II** (dashed lines) and **III** (continuous lines) are compared. (b) The view of K tunnel perpendicular to *c* axis. The K−K distances are 2.89 Å, and their coordinations geometry are square planar.

2.73 Å. For all Bi^{3+} ions, bond valence sums (BVS) listed in Table 2 are in good agreement with the expected values. K1 and K3 occupy corners of the columns and are surrounded by 10 O atoms. The K−O distances range from 2.70 to 3.22 Å, leading to BVS = 1.10 and 1.04 for K1 and K3, respectively. In the channels, the K2 atom is coordinated to eight O atoms at distances from 2.77 to 3.12 Å. The present K−O distances do not differ very much from those for K1 and K3 leading to BVS = 0.99. The disorder around S(4) tetrahedron mentioned above is supported by the overlarge values of isotropic or equivalent isotropic displacement parameters of O4b−4d. Admittedly, BVS calculations for S1−S4 sites also lead to +6.2−+7.1 as given in Table 2.

Compound III. The crystal structure of $[Bi_{8.73}K_{0.27}O_8][K_{1.54}(PO_4)_4]$ was solved in the *I*4/*m* space group (a = 13.977(2) Å, c = 5.7846(7) Å, and V = 1130.1(2) Å^3) with the final reliability factors R1 = 7.0%, wR2 = 7.56%. Its crystal structure is related to those of the fully ordered $[Bi_7K_2O_8][K(SO_4)_4]$ and of the modulated $[Bi_{10}(Bi_{\sim 0.5}Cd_{\sim 0.5})_8O_{16}](Bi_{0.6}Cd_{0.8})_2(PO_4)_8$[34] mentioned above. However, the present crystal structure is a pertinent example of a "fully disordered" prototype, in the sense that several subunits show statistic distribution over mixed K/Bi sites (edges) and partially occupied K channels. We note that diffraction patterns show no evidence of any ordering (extra spots) nor pseudo-ordering (diffuse streaks), similar to another disordered bismuth potassium phosphate, $[Bi_2(Bi_{1.56}K_{0.44})O_3]K_{0.88}(PO_4)_2$.[34] The refined atomic positions and anisotropic displacement parameters are given in Supporting Information Tables S8 and S9, respectively. The pertinent distances are listed in Supporting Information Table S10. The K/Bi disorder discussed below is at the origin of several overlarge thermal parameters due to local disorder, e.g., on connected SO_4 groups for instance.

The formula of the 1D-columns is $[Bi_{8.72}K_{0.27}O_8]^{+5}$ in which the site at the edges of the column is mixed and is refined to $[Bi_{0.72}K_{0.27}]$. For this refinement, due to the close Fourier difference peak, the full occupancy was restrained while K and Bi atomic coordinates were free-refined but restrained to equal thermal parameters. As for the occupancy of the interstitial K atoms, the initial refined occupancy was 0.73; however, it was finally fixed in the last cycles to 0.77 in order to keep the structure electroneutral, without significant increasing of structure reliability factors.

The lattices of compounds **II** and **III** could be related to each other via the following relationships: $\vec{a}_M \approx 2\vec{a}_T$, $\vec{b}_M \approx 2\vec{c}_T$, $\vec{c}_M \approx \vec{b}_T - \vec{a}_T$ (M, monoclinic **II**; T, tetragonal **III**) (Figure 6a). The reduced monoclinic cell of compound **II** V_M is larger than those of V_T of the tetragonal cell of compound **III** (V_M = 2388 Å^3 vs V_T = 2260 Å^3). Strikingly, it is in marked contrast to the

dx.doi.org/10.1021/ic501776h | Inorg. Chem. 2014, 53, 12058−12065

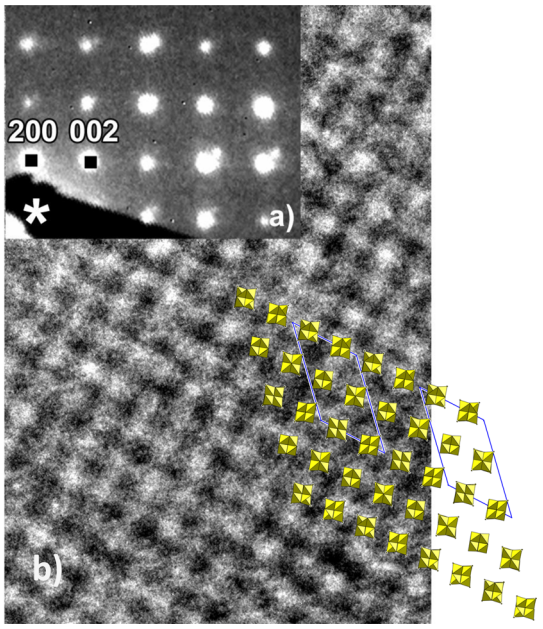

Figure 7. TEM images for compound **II**: (a) [010] electron diffraction zone axis pattern (EDZAP), (b) corresponding TEM image with the projected structure along *b*-axis. The white dots indicate the position of the $[Bi_7K_2O_8]^{7+}$ blocks.

comparison of respective volumes of SO_4 (1.54 Å^3, average of four SO_4 tetrahedra) versus PO_4 (V = 1.72 Å^3).[35] Apart from the different composition of the oxocentered framework, it is due to the different orientations of SO_4 delimiting the tunnels and their filling possibility.

CONCLUSION

The achievement of new inorganic compounds with either columnar 1D-units or porous 3D-network made of (OBi_4) tetrahedra remains rare, and only a few compounds have been reported to date.[1] With the parent structure being the 3D-fluorite-type with condensation of OBi_4 tetrahedra, after depletion of oxocentered tetrahedral, these units conserve one or more dimensions. We already discussed the analogy of 2 × 2 *Td* columns found in compounds **II** and **III** with recent compounds of the literature. In the case of porous frameworks (compound **I**), those reported in the literature mainly display channels with triangular sections of variable size filled by large halides such as Cl^-: $[Bi_{48}O_{58.64}][Ag_{4.78}Cl_{31.5}]_{channel}$,[36] $[Bi_6O_7F][Cl_3]_{channel}$,[37] and $[Bi_{12}O_{15}][Cl_6]_{channel}$[38] (Figure 7). Recently, three new other "multi-D" compounds owing such triangular pores concomitantly with infinite chloride layers were tackled, but compound **I** appears to be, to our knowledge, the first containing square sections of channels observed in 3D-Bi/O lattice. By comparison in the case of (OPb_4) tetrahedra, the parent structure is the layered litharge PbO structure, while the removal of OPb_4 generally preserves 2D-layers but porosity remains. Several compounds have been reported with rectangular or square sections such as shown in Figure 8. This figure displays porous layers of (a) $Pb_{10}O_7(SO_4)Cl_4(H_2O)$,[39] (b) $Pb_8O_5(OH)_2Cl_4$,[40] (c) $Pb_{47}O_{24}(OH)_{13}Cl_{25}(BO_3)_2(CO_3)$,[41] and (d) $Pb_{14}O_9(VO_4)_2Cl_4$,[42] with various section sizes. It follows that, in the context of the design of novel open structures in related chemical systems, the nature of Pb versus Bi cations in the main building blocks plays a key role in the final dimensionality of the crystal structure and could be used as a controlled tool. However, we note that, in using both Pb and Bi cations, we have recently reached a series of 2D-phases with Cl^- in the interleaves, in absence of any pores.[43,44]

ASSOCIATED CONTENT

Supporting Information

Crystallographic information in CIF format.

Tables for XRD analysis. This material is available free of charge via the Internet at http://pubs.acs.org.

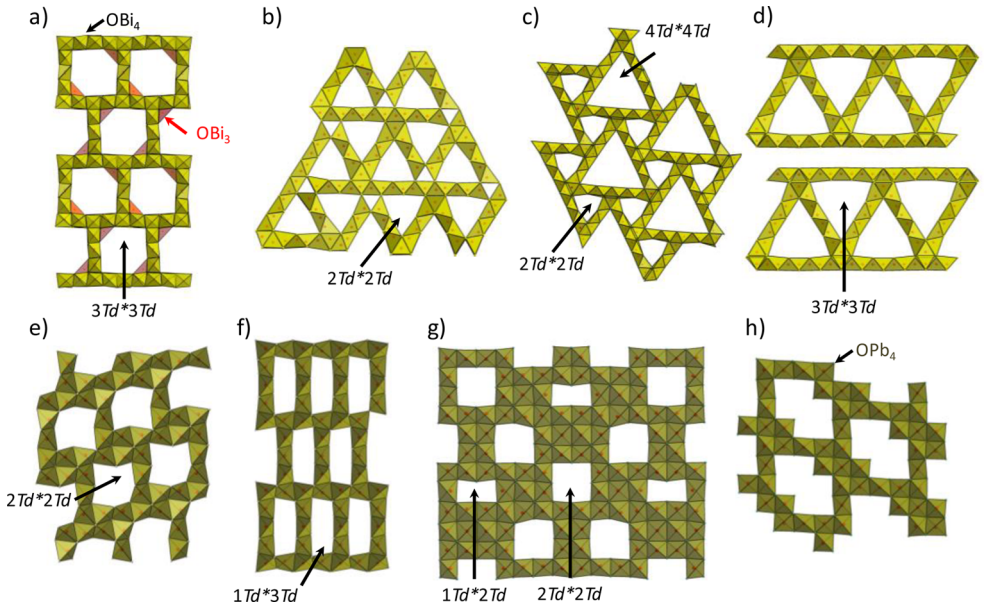

Figure 8. Variety of sections observed in lead and bismuth oxo compounds enhancing (a) 3*T**3*Td* in $[Bi_{12}O_{15}][Li_2(SO_4)_4]$, 2*T**2*Td* in (b) $[Bi_{12}O_{15}][Cl_6]$[38] and (c) $[Bi_{48}O_{58.64}][Ag_{4.78}Cl_{31.5}]$,[36] and (d) 3*T**3*Td* sections in $[Bi_6O_{7.5}]Cl_4Na_1$,[45] (e) 2*T**2*Td* in $Pb_{10}O_7(SO_4)Cl_4(H_2O)$,[39] (f) 1*T**3*Td* in $Pb_8O_5(OH)_2Cl_4$,[40] (g) association of 2*T**2Td and 1*T**3Td in $Pb_{47}O_{24}(OH)_{13}Cl_{25}(BO_3)_2(CO_3)$,[41] (h) and some oval-likes in $Pb_{14}O_9(VO_4)_2Cl_4$.[42]

dx.doi.org/10.1021/ic501776h | *Inorg. Chem.* 2014, 53, 12058−12065

AUTHOR INFORMATION

Corresponding Authors

*E-mail: marie.colmont@ensc-lille.fr. Phone: +33 (0) 3320336434.

*E-mail: olivier.mentre@ensc-lille.fr. Phone: +33 (0) 320337721.

Notes

The authors declare no competing financial interest.

ACKNOWLEDGMENTS

The Fonds Européeen de Développement Régional (FEDER), CNRS, Région Nord Pas-de-Calais, and Ministère de l'Education Nationale de l'Enseignement Supérieur et de la Recherche are acknowledged for funding the X-ray diffractometers. This work was carried out under the framework of the Multi-InMaDe project supported by the ANR (Grant ANR 2011-JS-08 003 01). The TEM facility in Lille (France) is supported by the Conseil Regional du Nord-Pas de Calais, and the European Regional Development Fund (ERDF).

REFERENCES

(1) Krivovichev, S. V.; Mentré, O.; Siidra, O. I.; Colmont, M.; Filatov, S. K. *Chem. Rev.* **2013**, *113*, 6459−6535.

(2) Takahashi, T.; Iwahara, H. *Mater. Res. Bull.* **1978**, *13*, 1447−1453.

(3) Takahashi, T.; Iwahara, H. *J. Appl. Electrochem.* **1973**, *3*, 65−72.

(4) Spinolo, G.; Tomasi, C. *Powder Diffr.* **1997**, *12*, 16−19.

(5) Chiodelli, G.; Magistris, A.; Spinolo, G.; Tomasi, C.; Antonucci, V.; Giordano, N. *Solid State Ionics* **1994**, *74*, 37−45.

(6) Ling, C. D.; Thompson, J. G.; Withers, R. L.; Schmid, S. *J. Solid State Chem.* **1999**, *142*, 33−40.

(7) Francesconi, M. G.; Kirbyshire, A. L.; Greaves, C.; Richard, O.; Van Tendeloo, G. *Chem. Mater.* **1998**, *10*, 626−632.

(8) Crumpton, T. E.; Greaves, C. *J. Mater. Chem.* **2004**, *14*, 2433.

(9) Smirnov, V. *Solid State Ionics* **2003**, *156*, 79−84.

(10) Datta, R. K.; Meehan, J. P. *Z. Anorg. Allg. Chem.* **1971**, *383*, 328−337.

(11) Kashida, S.; Hori, T. *J. Solid State Chem.* **1996**, *122*, 358−363.

(12) Watanabe, A.; Kitami, Y. *Solid State Ionics* **1998**, *113−115*, 601−606.

(13) Lee, S. L.; Lee, C. K.; Sinclair, D. C.; Chong, F. K.; Halim, S. A.; Yap, T. *Malays. J. Chem.* **2005**, *7*, 1−10.

(14) Darriet, J.; Launay, J. C.; Zúniga, F. J. *J. Solid State Chem.* **2005**, *178*, 1753−1764.

(15) Labidi, O.; Drache, M.; Roussel, P.; Wignacourt, J.-P. *Solid State Sci.* **2008**, *10*, 1074−1082.

(16) Kuang, X.; Payne, J. L.; Farrell, J. D.; Johnson, M. R.; Evans, I. R. *Chem. Mater.* **2012**, *24*, 2162−2167.

(17) Kozin, M. S.; Colmont, M.; Endara, D.; Aliev, A.; Huvé, M.; Siidra, O. I.; Krivovichev, S. V.; Mentré, O. *J. Solid State Chem.* **2013**, *199*, 123−128.

(18) Colmont, M.; Endara, D.; Aliev, A.; Terryn, C.; Huvé, M.; Mentré, O. *J. Solid State Chem.* **2013**, 266−272.

(19) Lü, M.; Colmont, M.; Kabbour, H.; Colis, S.; Mentré, O. *Inorg. Chem.* **2014**, *53*, 6969−6978.

(20) Margulis, E. V.; Grishankina, N. S.; Kopylov, N. I. *Russ. J. Inorg. Chem.* **2003**, 79.

(21) Aurivillius, B. *Acta Chem. Scand., Ser. A* **1987**, *41*, 415.

(22) Aurivillius, B. *Acta Chem. Scand.* **1988**, *42*, 95−110.

(23) Matsuzaki, R.; Sofue, A.; Masumizu, H.; Saeki, Y. *Chem. Lett.* **1974**, 737−740.

(24) Harwig, H. A. *Z. Anorg. Allg. Chem.* **1978**, *444*, 151−166.

(25) Logemann, C.; Kleineberg, H.; Ohlert, J.; Wickleder, M. S. *Z. Anorg. Allg. Chem.* **2013**, *639*, 2796−2803.

(26) *SAINT: Area-Detector Integration Software*; Siemens Industrial Automation, Inc.: Madison, WI, 1996.

(27) *SADABS: Area-Detector Absorption Correction*; Siemens Industrial Automation, Inc.: Madison, WI, 1995.

(28) Stadelmann, P. *JEMS: EMS Java Version*; CIME-EPFL: Lausanne, 1999

(29) Palatinus, L.; Chapuis, G. *J. Appl. Crystallogr.* **2007**, *40*, 786−790.

(30) Petricek, V.; Dusek, M.; Palatinus, L. *Jana2006. The Crystallographic Computing System*; Institute of Physics: Praha, Czech Republic, 2006.

(31) Spek, A. L. *Acta Crystallogr., Sect. D* **2009**, *65*, 148−155.

(32) Brown, I. D. *Chem. Rev.* **2009**, *109*, 6858−6919.

(33) Aliev, A.; Endara, D.; Huvé, M.; Colmont, M.; Roussel, P.; Delevoye, L.; Tran, T. T.; Halasyamani, P. S.; Mentré, O. *Inorg. Chem.* **2014**, *53*, 861−871.

(34) Sheldrick, G. M. *SHELXTL NT, Program Suite for Solution and Refinement of Crystal Structure, Version 5.1*; Bruker Analytical X-ray Systems: Madison, WI.

(35) Dolomanov, O. V.; Bourhis, L. J.; Gildea, R. J.; Howard, J. A. K.; Puschmann, H. *J. Appl. Crystallogr.* **2009**, *42*, 339−341.

(36) Aurivillius, B.; Albertsson, J.; Svensson, G.; Eberson, L.; Krogsgaard-Larsen, P.; Maartmann-Moe, K.; Wold, S. *Acta Chem. Scand.* **1990**, *44*, 111−122.

(37) Hopfgarten, F. *Acta Crystallogr., Sect. B* **1975**, *31*, 1087−1092.

(38) Hopfgarten, F. *Acta Crystallogr., Sect. B* **1976**, *32*, 2570−2573.

(39) Welch, M. D.; Cooper, M. A.; Hawthorne, F. C.; Criddle, A. J. *Am. Mineral.* **2000**, *85*, 1526−1533.

(40) Krivovichev, S.; Burns, P. C. *Can. Mineral.* **2006**, 515−522.

(41) Krivovichev, S. V.; Turner, R.; Rumsey, M.; Siidra, O. I.; Kirk, C. A. *Mineral. Mag.* **2009**, *73*, 103−117.

(42) Cooper, M.; Hawthorne, F. C. *Am. Mineral.* **1994**, *79*, 550−554.

(43) Aliev, A.; Olchowka, J.; Colmont, M.; Capoen, E.; Wickleder, C.; Mentré, O. *Inorg. Chem.* **2013**, *52*, 8427−8435.

(44) Lü, M.; Aliev, A.; Olchowka, J.; Colmont, M.; Huvé, M.; Wickleder, C.; Mentré, O. *Inorg. Chem.* **2014**, *53*, 528−536.

(45) Sillén, L. G. *Z. Anorg. Allg. Chem.* **1939**, *242*, 41−46.